Selected aspects of blood flow simulations in arteries

Ryszard Białecki*[a], Wojciech Adamczyk[a], Ziemowit Ostrowski[a]

[a] Silesian University of Technology, Department of Thermal Technology, Faculty of Energy and Environmental Engineering, Konarskiego 22, 44-100 Gliwice, Poland
*Corresponding author email: ryszard.bialecki@polsl.pl

Abstract

This article discusses selected aspects of modelling blood flow in the arteries. The method of reproducing the variable-in-time geometry of coronary arteries is given based on a sequence of medical images of different resolutions. Within the defined shapes of the arteries, a technique of generation of numerical meshes of the same topology is described. The boundary conditions and non-Newtonian rheological models used in blood flow are discussed, as well as the description of blood as a multiphase medium. The work also includes a discussion of tests on the phantom of the carotid artery for the accuracy of measurements made using ultrasonography.

Keywords: Blood flow; CFD; Coronary arteries; Boundary conditions; Blood rheology; Blood as a multiphase medium

1. Introduction

Blood flow is fundamental to the functioning of the human body. It is involved in several physiological processes that are necessary for life:

1. Transport of oxygen: Blood is responsible for the transport of oxygen from the lungs to all tissues of the body.
2. Transfer of nutrients and removal of waste products: It also transports nutrients produced as a result of the digestion of food to cells throughout the body and helps to remove metabolic byproducts, including carbon dioxide from cells.
3. Pressure regulation: The heart and blood vessels regulate blood flow and pressure. This is necessary to ensure that blood reaches all parts of the body.
4. Temperature regulation: Blood intensifies the heat exchange between the body and the surroundings.

5. Immune system support: The leukocytes contained in the blood defend the body against infections, viruses, and other pathogens.
6. Distribution of hormones: Hormones, produced by various glands that regulate physiological processes, are transported in the bloodstream to the target organs and tissues.
7. Clotting and wound healing: The healing process is initiated by platelets that initiate clot formation to prevent excessive bleeding.
8. Maintaining the pH and electrolyte balance: Blood contains buffers that can handle changes in pH and electrolytes (such as sodium, potassium, and calcium) that are crucial for different physiological functions.

The paper describes some aspects of modelling blood flow in the arteries that have been developed by the authors of this paper within recent research projects. The article does not de-

Białecki R., Adamczyk W., Ostrowski Z.

Nomenclature

A – cross-sectional area, m^2
D – vessel diameter, mm
E – Young modulus, GPa
f – frictional force
h – wall thickness, mm
k – constant in Quemada viscosity
ΔL – distance between the measurement points, mm
p – pressure, mmHg
Q – volumetric flow, m^3/s
R – tube radius, mm
S – cross-sectional area, m^2
t – time, s
U – cross-sectional averaged velocity, m/s
u – local velocity, m/s
Wo – Womersley number

Greek symbols

γ – shear rate

μ – dynamic viscosity, Pa·s
ν – kinematic viscosity, m^2/s
ρ – blood density, kg/m^3
τ – wall shear stress, Pa
ω – circular frequency of the flow changes

Subscripts and Superscripts

c – critical shear rate
p – plasma
w – wall

Abbreviations and Acronyms

CTA – Computed Tomography Angiography
FSI – Fluid-Structure Interaction
ICA – Invasive Coronary Angiography
MB – Myocardial Bridge
LV – Left heart Ventricle
USG – Ultrasonography
RBC – Red Blood Cells
WSS – Wall Shear Stress

scribe a complete research program but focuses on some important aspects of blood flow that the team encountered during ongoing research projects. Emphasis was placed on the issues that caused the team special difficulties. The article presents ready-made solutions to some problems but also shows possible approaches not yet implemented in the practice of the team. A comprehensive overview of the applications of CFD in hemodynamics can be found in references [1, 2].

The methods and examples discussed in the article concern the arteries of the systemic circulatory system. The walls of the arteries, unlike the walls of the veins, experience significant differences in cyclic pressure caused by heart contractions.

The characteristic features to be considered in flow simulations in the arteries are:

- complex geometry and numerous arterial branches,
- pulsatile, cyclic nature of pressure and flow variability,
- deformation of the vessel walls,
- non-Newtonian rheology,
- nonstandard boundary conditions.

2. Dimensionality of the model

The total length of the arteries in the human body is estimated to be between 100 000 and 160 000 km. The development of a model of geometry of the entire circulatory system is not realistic.

There are models of blood circulation in the human body based on one-dimensional models and the restriction of geometry to larger-diameter vessels. An example of such an approach is the open code STARFiSh developed at NTNU Trondheim [3]. The code is based on a solution of a system of first-order differential equations with partial derivatives:

$$\frac{\partial A}{\partial t} + \frac{\partial Q}{\partial x} = 0, \tag{1}$$

$$\frac{\partial Q}{\partial t} + \frac{\partial \left(\alpha \frac{Q^2}{A} \right)}{\partial x} = -\frac{A}{\rho} \frac{\partial p}{\partial x} + \frac{f}{\rho}. \tag{2}$$

where A is the cross-sectional area, Q is the volumetric flow, p is the pressure assumed constant over the cross-section, ρ is the density of blood, f is the frictional force, α accounts for nonlinearity in the cross-sectional integration of the local velocity u:

$$\alpha(t, x) = \frac{1}{AU^2} \int_S u^2 dS, \tag{3}$$

where U is the cross-sectional averaged velocity.

It has been recognized that the distribution of the shear stresses on the wall of the vessel determines the tendency of deposition of atherosclerotic plaques at the internal layer (endothelium) of the vessel [4]. At the level of histopathology, endothelial cells change their shape from elongated to nearly round and their state from atheroprotective to atherogenic [5].

Equations (1–2) are very useful to simulate the blood flow within the whole body. However, 1D models do not provide details of the blood flow pattern in the vessel, specifically the shear stress at the wall. The latter can be determined only using 2D or 3D models, preferably in time-dependent geometry. 2D models are applied to reduce computational time; in most cases, these papers assume axisymmetry of the geometry [6]. Both 2D and 3D models are based on solutions of the Navier-Stokes equations (mass and momentum conservation). The simplest cases do not account for pulsatile flow using average or extremum flow conditions [7].

More sophisticated approaches use time-dependent boundary conditions (pressure of flow) but neglect the deformation of the walls of the vessels during the cardiac cycle. For most of the major healthy arteries, the vessel diameter changes during the cardiac cycle are approximately 5–10% [8]. Therefore, there are numerous articles in which the walls of the vessels are treated as rigid [9].

The next complexity involves accounting for the periodic deformation of the vessels. 3D simulations where the flexibility of the walls is accounted for are computationally demanding compared to rigid wall modelling. In this case, two techniques are available when:

- the change in geometry is known from medical imaging techniques such as noninvasive coronary CT (CCTA), invasive coronary angiography (ICA), and intravascular ultrasound (IVUS) [10];
- the deformation of the vessels is obtained by applying the fluid-structure interaction where the stress/stress field in the walls is coupled with the blood flow pattern [11].

The remaining portion of the paper is devoted to 3D models.

3. Retrieving the time-dependent geometry. Case of coronary arteries

Coronary arteries are located on the surface of the heart muscle (myocardium). As a result, these arteries are not squeezed at systole and can transport oxygen and nutrients to the heart muscle. Arteries are permanently attached to the myocardium whose volume and shape change during the cardiac cycle causing variations in artery length and curvature. In addition, pressure pulsations generated by the contraction of the left ventricle generate changes in the lumen of the vessel.

The geometry of the coronary artery can even be more complex in the presence of the so-called myocardial bridge (MB) when muscle bands overlay a segment of the coronary artery. This condition is mostly asymptomatic, however, in some cases, it may result in myocardial ischemia, angina, acute coronary syndrome, etc. The presence of MB causes an oscillation in blood flow that results in a deposition of the atherosclerotic plaque proximal (before the inflow) on MB.

The geometry of the vessel can be retrieved by several modalities. The medical images that were used in the paper were acquired at the Silesian Centre of Heart Diseases using angio-computed tomography.

The raw data used to retrieve the geometry of the coronary arteries consisted of a set of ECG-gated angio-CT images recorded every 10% of the time of the cardiac cycle. To reduce the harmful effect of the X-rays on the patient, the radiation dose was not only low but also modulated within the cycle. As a result, the resolution of these packages of images was low. Additional high-resolution images have been taken separately for diastole and systole. The total set consisted thus of images of various resolutions and quality, specifically 10 images of 256×256 resolution and 2 images (diastole/systole) of 512×512 resolution. The images have been recorded by a 128-slice dual-source computed tomography scanner (SOMATOM Definition Flash, Siemens Healthineers, Forchheim, Germany) using beam collimation 2×64 mm $\times$ 0.6 mm, slice thickness of 1.5 mm and reconstruction interval of 0.5 mm. Figure 1 shows an example of a raw image.

The set of images requires intensive processing consisting of:

1. segmentation of low-resolution images (extraction of coronary artery shapes from 3D image data);
2. co-registration of the low-resolution images corresponding to subsequent time instants of the cardiac cycle (the process of transforming images into one coordinate system). The result is a set of nonlinear transformations showing the transition between subsequent images;

3. segmentation of the high-resolution data and generation of a 3D surface in STL format;
4. smoothing the obtained in step 3 STL surface;
5. generation of CFD mesh in the smoothed object obtained in step 4;
6. transformation of the mesh obtained in step 5 using the nonlinear transformation resulting from step 2 (co-registration).
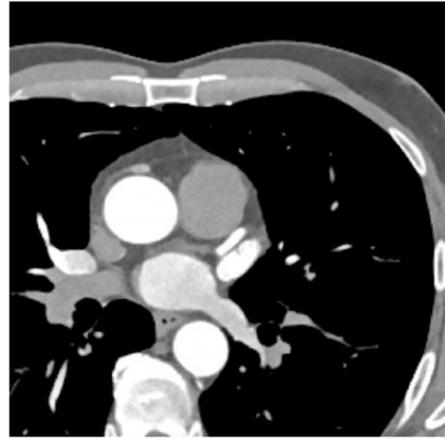

Fig. 1. An example of a raw high-resolution image.

Segmentation of medical images (steps 1 and 3) was carried out using the active contour method with threshold-based pre-segmentation implemented in the ITK SNAP package [12]. The theory behind this method is to find the close contours by solving the equation:

$$\frac{\partial C(u,v,t)}{\partial t} = \vec{F} \cdot \vec{n} , \qquad (4)$$

where: C – closed contour parametrized by u, v, t with u and v denoting the local coordinates and t – time, $\vec{F}$ $\vec{n}$ – the sum of internal and external forces acting on the contour in the normal direction: internal forces associated with the curvature, external with the gradient of the imaged intensity.

The co-registration process consists of three steps: rigid body movement, affine transformation, and nonlinear transformation based on diffeomorphism. These transformations are executed using the ANTs package [13].

The raw 3D surface retrieved from the high resolution data was smoothed using the GeoMagic software [14]. The CFD mesh generation is performed using a standard Fluent Ansys mesher [15]. The nodes of the CFD mesh generated in step 5 are projected using the transformation matrix obtained in step 5 onto every low-resolution object. Based on this surface mesh, the volumetric mesh at each step is generated. The advantage of the proposed method is the generation of a CFD mesh of the same topology at each instant of time. Due to this, the interpolation errors between grids are avoided, the mesh morphing utility can be used directly, and the CFD calculation time is reduced.

The scheme of generation of the geometry of the coronary arteries is shown in Fig. 2. The resulting geometries at 30, 50, 70 and 90% of the cardiac cycle are shown in Fig. 3.
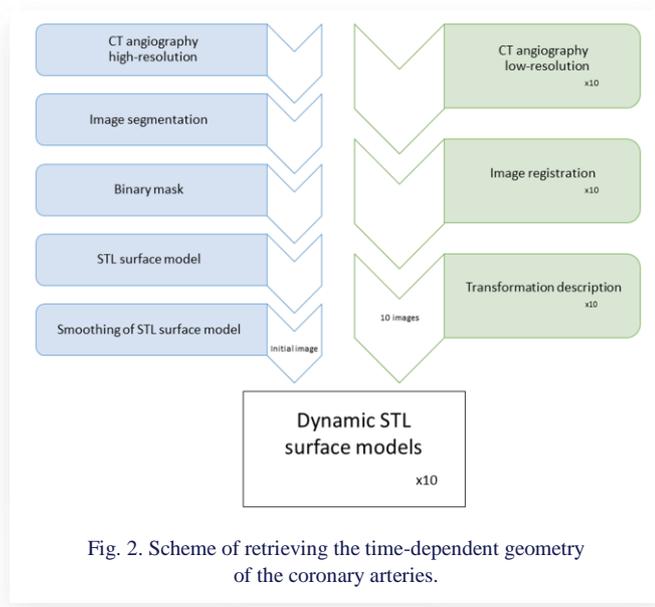
Fig. 2. Scheme of retrieving the time-dependent geometry
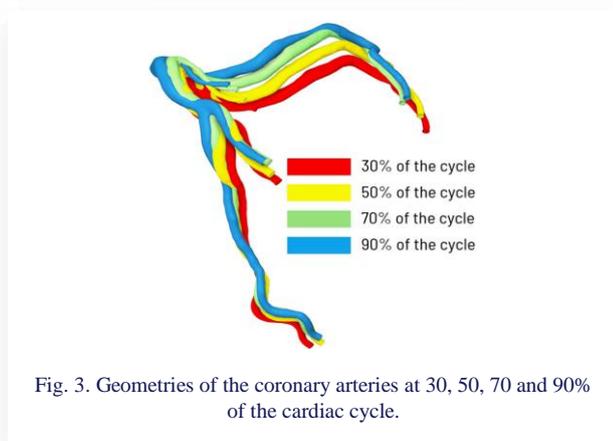of the coronary arteries.

Fig. 3. Geometries of the coronary arteries at 30, 50, 70 and 90%
of the cardiac cycle.

4. Measurement of the phantom deformation of the carotid artery

The stiffness of the arteries is a measure of the rigidity of the arterial walls. This property changes with age due to remodeling of the artery wall structure where elastic elastin fibers are replaced by stiffer collagen ones. Increased stiffness is a condition that can have several serious implications for overall well-being. Increased stiffness may result in:

- Hypertension that results from the superposition of the main pressure pulse generated by the systole of the left heart ventricle (LV) and the wave reflected from the bifurcations of the arteries;

- Thickening of the heart muscle (LV hypertrophy) due to the increased workload of the left ventricle resulting from its increased workload contributing to the increased risk of heart failure;

- Reduced blood flow to organs due to the reduced ability of the blood vessels to constrict and dilate;

- Damage of end organs such as kidneys, eyeballs and brain caused by the reduced ability to dump the pulsation of the blood pressure.

The stiffness of the blood vessels is assessed by measuring the pulse wave velocity PWV obtained from the time that elapses between pressure peaks in two arteries (usually carotid and femoral). This value is obtained using the Moens-Kortweg equation [16]:

$$PWV = \frac{\Delta L}{\Delta t} = \sqrt{\frac{Eh}{D\rho}}, \qquad (5)$$

where: E – Young modulus of the wall, h – wall thickness, D – vessel diameter, ρ – blood density, ΔL – distance between the measurement points along the blood vessel, Δt – time that elapsed between the pressure peaks at measurement points.

Equation (5) gives the mean values of the stiffness of the vessel wall between the pressure measurement points. The project aimed to determine the local stiffness of the carotid artery wall by solving an inverse problem of blood flow in a deforming conduit (solving the fluid-structure interaction (FSI) problem) based on the measured deformation of the walls. The latter was measured using the ultrasound scanner.

The key issue was to determine the precision of the ultrasonography (USG) measurements and the validation of the FSI model based on measurements performed on a phantom undergoing a load similar to the carotid artery. For this purpose, a phantom was built in which pressure pulsations mimicking the work of the heart are produced by a pump, and the deformations of the flexible tube are measured in two perpendicular planes by high-resolution digital cameras. Parallel to these deformation measurements, deformation is measured with a USG scanner. Figure 4 shows the scheme of the experimental rig. The photo of the rig is shown in Fig. 5. The comparison of the camera and USG scanner uncertainties in measured displacements is shown in Fig. 6. As can be seen, the ultrasound-derived displacements exhibit good agreement (mean difference of 0.0113 mm) in comparison with the camera-generated data.
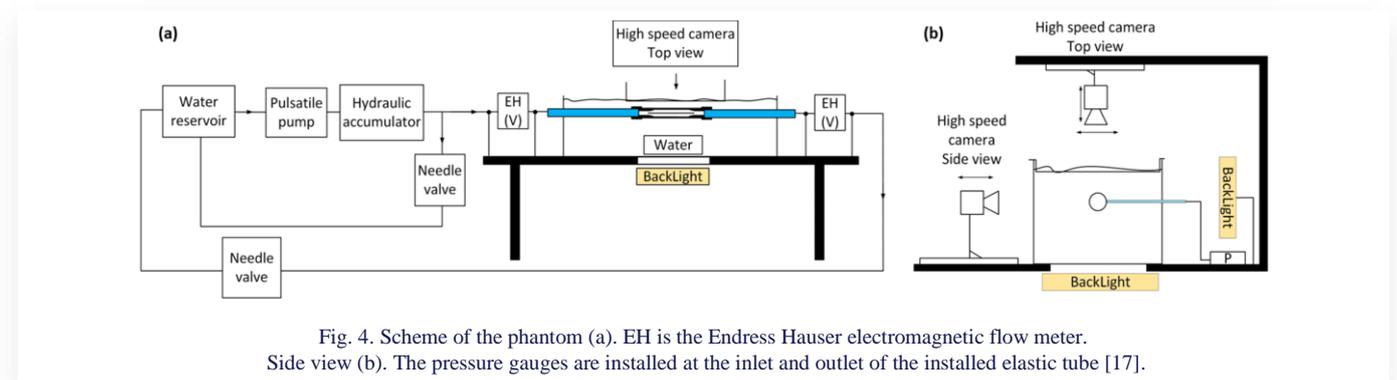

Fig. 4. Scheme of the phantom (a). EH is the Endress Hauser electromagnetic flow meter.
Side view (b). The pressure gauges are installed at the inlet and outlet of the installed elastic tube [17].
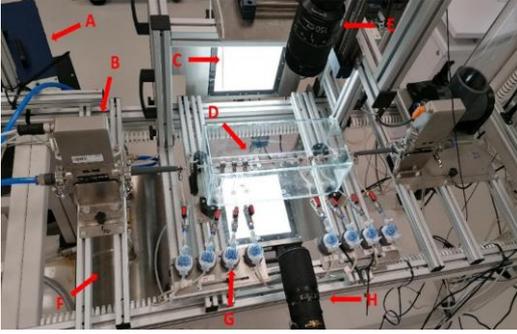
Fig. 5. Photo of the test rig: A – periodic pump, B – flowmeter, C – backlight, D – arterial phantom, E – top camera (MIRO), F – reservoir tank, G – pressure transducers, H – side camera (VEO) [17].
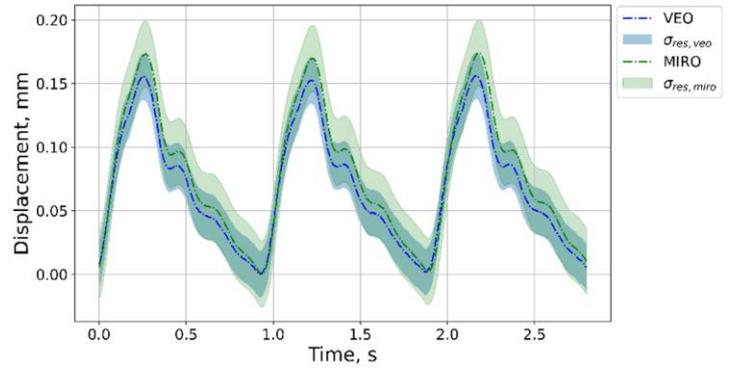

Fig. 6. Comparison of displacements recorded by both cameras with uncertainty represented by overlaid shaded areas. In both cases, uncertainty is characterized as dr el,cam ± σres,cam [17].

5. Boundary conditions

In the case of 3D simulations, simulation of blood flow in the entire cardiovascular system would lead to a prohibitively long calculation time. Therefore, the computational area is limited to a small portion of the circulatory system with at least one inlet and one outlet defined at fictitious surfaces closing the truncated vessel. To obtain the blood flow solution of the Navier-Stokes equations, unambiguous boundary conditions should be specified at these fictitious surfaces. These boundary conditions are formulated in terms of velocity (mass flow), pressure, or a relationship between these two parameters. It should be stressed that the fluid mechanics outflow conditions commonly used cannot be used in blood flow simulations. Such boundary conditions can be applied only in the case of fully developed velocity profiles that correspond to flow in a long, constant cross-section.

Moreover, although the flow in the arteries is, with very few exceptions, laminar, the velocity profile in the arteries is not parabolic. It is the pulsating blood flow generated by the contraction of the left ventricle that distorts the velocity profile. The resulting distribution of the velocity is, for the idealized case of flow in a stiff, constant cross-section tube, governed by the Womersley number defined as:

$$\text{Wo} = R\sqrt{\frac{\omega}{\nu}}, \qquad (6)$$

where: R – tube radius, ω – circular frequency of the flow changes, ν – kinematic viscosity. Figure 7 shows the speed profiles for different Womersley numbers.

The boundary conditions can be defined using three approaches:

- measurements (patient-specific data),
- statistics (population data),
- estimates based on physiological assumptions and models.

It is recommended to use, whenever applicable, the first option and define the velocity or pressure. Statistical data cannot be patient-specific and only represent the general population. Inflow and outflow conditions can also be assessed using theories such as Murray's law [19] which defines the link between mass flow rate and vessel diameter, or the theory of constant wall shear stress [20]. Alternatively, the interaction of the computa-

tional domain with the remaining part of the cardiovascular system can be addressed using the multi-scale approach. The idea is to couple the 3D model with the 1D [21] or 0D [22] model describing the behaviour of the peripheral vascular system. The latter is usually based on the hydraulic/electric analogy with flow resistance resulting in pressure drop and capacitance describing vascular compliance. The lower-order model is described by an ordinary differential equation whose parameters, describing the behaviour of the vascular system outside of the 3D model, are not easy to determine. Implementation of this type of nonlinear boundary condition leads to an iterative procedure and often requires stabilization.
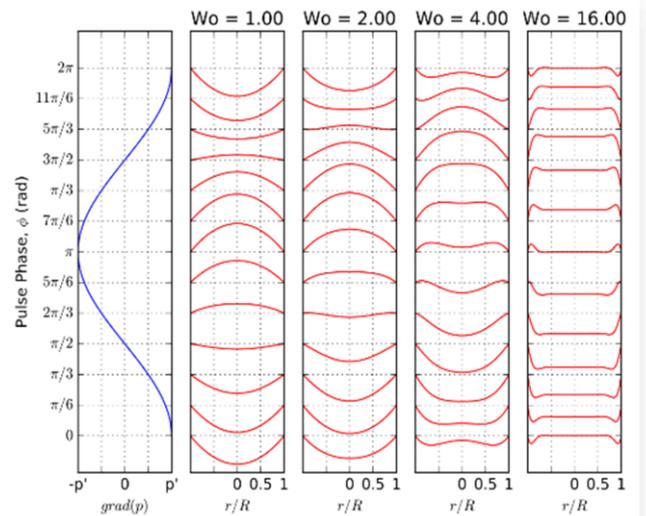

Fig. 7. Four pulsatile flow profiles in a straight tube. The first graph (in blue) shows the pressure gradient as a cosine function, and the other graphs (in red) show dimensionless velocity profiles for different Womersley numbers [18].

5.1. Velocity boundary conditions

In some cases, blood speeds can be measured using non-invasive methods such as the Doppler technique associated with ultrasound, magnetic resonance imaging and computed tomography angiography (CTA) (which requires contrast). Invasive methods

include arterial catheterization, a method that requires the introduction of a catheter into an artery, and rather rarely used electromagnetic flowmetry. The latter consists of measuring the generated voltage induced in coils placed near a blood vessel immersed in a variable. magnetic field.

5.2. Pressure Boundary Conditions

Non-invasive pressure measurement can be carried out at arteries located close to the surface of the body (carotid, radial, femoral) using the applanation tonometer technique [23, 24]. Pressure can be measured by invasive arterial catheterization.

6. Wall shear stress and oscillatory shear stress index

The deposition of atherosclerotic plaque on the walls of arteries depends on the wall shear stress (τ_w, WSS). Typically, the onset of plaque occurs at low τ_w locations while a high WSS prevents plaque deposition [4]. Another parameter that indicates plaque deposition is the oscillatory shear stress index OSI defined as [25]:

$$OSI = \frac{1}{2}\left(1 - \frac{|\int_0^T \tau_w dt|}{\int_0^T |\tau_w| dt}\right) \qquad (6)$$

Figure 8 shows the distribution of both indices in the left ascending coronary artery. The results have been obtained for the inflow condition: pulsatile pressure, and the outflow condition: mass distribution between outlets based on the Murray law (including accumulation in the volume of the arteries).
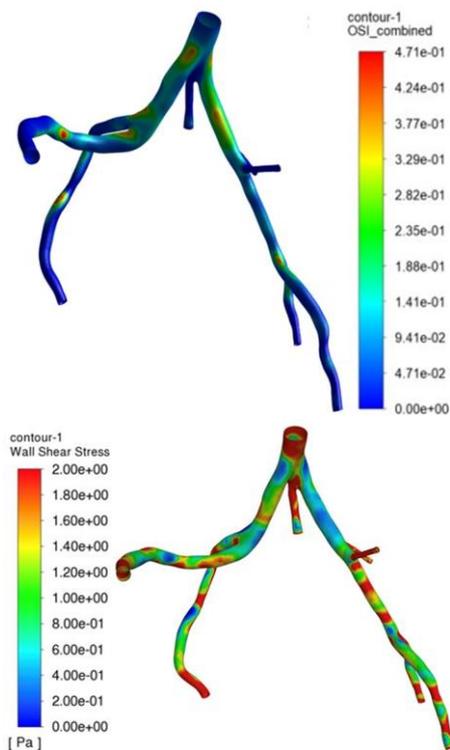

Fig. 8. Oscillatory shear stress index (top) and wall shear stress (bottom) for the maximum flow [26].

7. Rheology of blood

Blood is a non-Newtonian, multiphase fluid with cellular elements: red blood cells (RBC), white blood cells and platelets suspended in plasma. The latter is an aqueous solution containing organic molecules, proteins and salts. Plasma and red blood cells (erythrocytes) play a dominant role in the definition of the viscosity of blood. At low shear rates, the aggregation of RBC occurs accompanied by increased blood viscosity [27].

There are two possible approaches to account for the non-Newtonian properties of blood. The first is the usage of nonlinear constitutive laws for viscosity where the blood is treated as a one phase fluid. The second is to treat blood as a multiphase medium.

The most popular are [28]:
Carreau:

$$\mu = \mu_\infty + (\mu_0 - \mu_\infty[1 + (\lambda\gamma^2]^{\frac{n-1}{2}}), \qquad (7)$$

Casson:

$$\mu = \left(\sqrt{\mu_c} + \sqrt{\tau_c/\gamma}\right)^2, \qquad (8)$$

Quemada:

$$\mu = \mu_p(1 - \frac{1}{2}\frac{k_0 + k_\infty\sqrt{\frac{|\gamma|}{\gamma_c}}}{1 + \sqrt{\frac{|\gamma|}{\gamma_c}}}\phi)^{-2}, \qquad (9)$$

where γ is the shear rate and the remaining variables are constants, whose values can be found in [29].

Figure 9 shows the velocity contours corresponding to different instants of the cardiac cycle obtained using various rheological models [30] obtained for one velocity inlet and four pressure outlets, the numerical mesh consisting of 1.3 million cells.

8. Blood as a multiphase medium

When using non-Newtonian constitutive laws, blood is treated as a homogeneous liquid of viscosity that depends on the shear rate. An alternative approach is to take into account the presence of granular phases (blood cells) immersed in a liquid (plasma). The two most popular approaches are known as Euler-Euler and Euler-Lagrange. In the former, the Navier-Stokes equations for plasma are solved in the Eulerian coordinate frame. The granular phases are also modelled as fluids with appropriately defined properties and solved in the Euler coordinate frame. Both plasma and granular phases are then as interpenetrating continua.

In the Euler-Lagrange approach, first the plasma is solved separately in Eulerian coordinates, and then the fate of the granular phase is traced in the Lagrangian coordinates frame. As the volume fraction of the blood cells is high, the interactions (collisions) between the tranced cells should be accounted for. This requires a solution of an additional set of equations based on the kinetic theory of granular flow [31].

Figure 10 shows the results of simulations of blood flow in the aorta with coarctation (congenital narrowing) obtained by the Euler–Euler technique for the inlet pressure conditions and the boundary conditions of the 3-element Windkessel outlet [32].
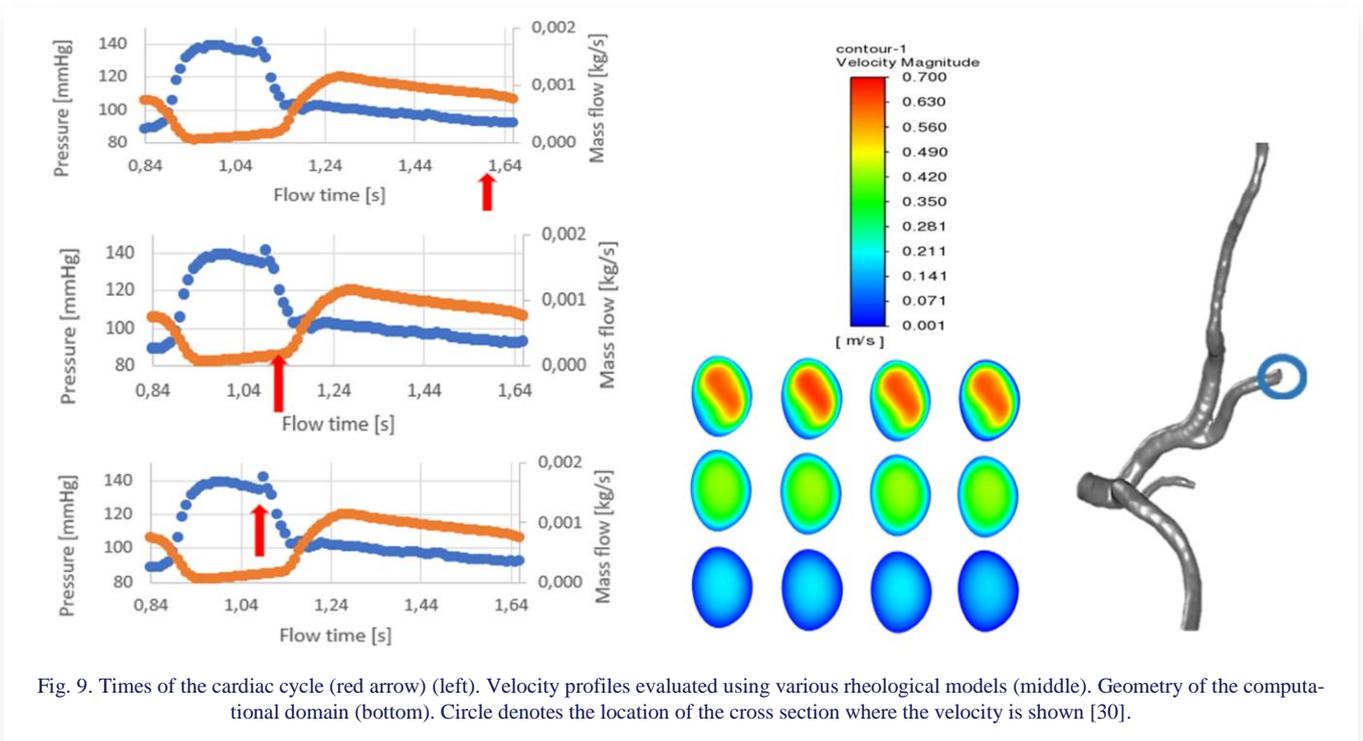
Fig. 9. Times of the cardiac cycle (red arrow) (left). Velocity profiles evaluated using various rheological models (middle). Geometry of the computational domain (bottom). Circle denotes the location of the cross section where the velocity is shown [30].
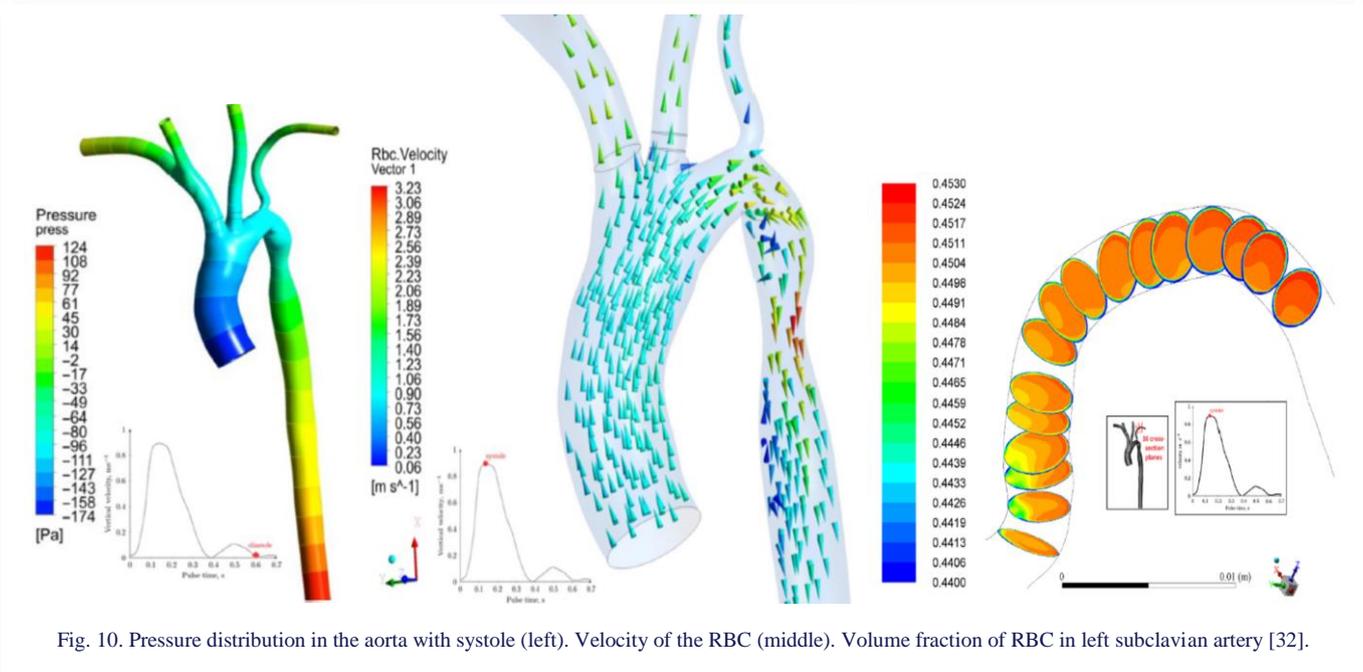

Fig. 10. Pressure distribution in the aorta with systole (left). Velocity of the RBC (middle). Volume fraction of RBC in left subclavian artery [32].

The results (see Fig. 9) confirm the presence of the Fhraeus-Lindqvist effect resulting from the movement of the RBC to the centre of the vessel leaving plasma near the wall [33].

9. Conclusions

CFD can be used successfully to simulate blood flow in the arteries. Reliable simulation results are based on the restoration of vessel geometry, which requires the processing of medical images obtained using tomographic modalities. The difficulties encountered in these activities result from the variability of images over time. The article shows a method that allows not only to reproduce such shapes but also to generate numerical grids with the same topology in subsequent time steps. Difficulties in blood flow simulations are also caused by the proper definition of boundary conditions and non-Newtonian blood rheology. An overview of the types of boundary conditions and rheological models encountered and examples of their application are given.

Acknowledgements

References

[1] Morris, P.D., Narracott, A., von Tengg-Kobligk, H., Silva Soto, D.A., Hsiao, S., Lungu, A., Evans, P., Bressloff, N.W., Lawford, P.V., Hose, D.R., & Gunn, J. P. (2016). Computational fluid dynamics modelling in cardiovascular medicine. *Heart (British Cardiac Society)*, 102(1), 18–28. doi: 10.1136/heartjnl-2015-308044

[2] Gijsen, F., Katagiri, Y., Barlis, P., Bourantas, C., Collet, C., Coskun, U., Daemen, J., Dijkstra, J., Edelman, E., Evans, P., van der Heiden, K., Hose, R., Koo, B.-K., Krams, R., Marsden, A., Migliavacca, F., Onuma, Y., Ooi, A., Poon, E., & Serruys, P. (2019). Expert recommendations on the assessment of wall shear stress in human coronary arteries: existing methodologies, technical considerations, and clinical applications. *European Heart Journal*, 40(41), 3421–3433. doi: 10.1093/eurheartj/ehz551

[3] Hellevik L.R., & Sturdy J. https://www.ntnu.no/starfish [accessed 20 Nov. 2023].

[4] Zhou, M., Yu, Y., Chen, R., Liu, X., Hu, Y., Ma, Z., Gao, L., Jian, W., & Wang, L. (2023). Wall shear stress and its role in atherosclerosis. *Frontiers in Cardiovascular Medicine*, 10, 1083547. doi: 10.3389/ fcvm.2023.1083547

[5] Malek, A.M. (1999). Hemodynamic shear stress and its role in atherosclerosis. *JAMA: The Journal of the American Medical Association*, 282(21), 2035. doi: 10.1001/jama.282.21.2035

[6] Katz, S., Caiazzo, A., Moreau, B., Wilbrandt, U., Brüning, J., Goubergrits, L., & John, V. (2023). Impact of turbulence modeling on the simulation of blood flow in aortic coarctation. *International Journal for Numerical Methods in Biomedical Engineering*, 39(5), 3695. doi: 10.1002/cnm.3695

[7] Bordones, A.D., Leroux, M., Kheyfets, V.O., Wu, Y.A., Chen, C.Y., & Finol, E.A. (2018). Computational fluid dynamics modeling of the human pulmonary arteries with experimental validation. *Annals of Biomedical Engineering*, 46(9), 1309–1324. doi: 10.1007/s10439-018-2047-1

[8] Taylor, C.A., Hughes, T.J.R., & Zarins, C.K. (1998). Finite element modeling of blood flow in arteries. *Computer Methods in Applied Mechanics and Engineering*, 158(1–2), 155–196. doi: 10.1016/s0045-7825(98)80008-x

[9] Gharahi, H., Zambrano, B.A., Zhu, D.C., DeMarco, J.K., & Baek, S. (2016). Computational fluid dynamic simulation of human carotid artery bifurcation based on anatomy and volumetric blood flow rate measured with magnetic resonance imaging. *International Journal of Advances in Engineering Sciences and Applied Mathematics*, 8(1), 46–60. doi: 10.1007/s12572-016-0161-6

[10] Decroocq, M., Frindel, C., Rougé, P., Ohta, M., & Lavoué, G. (2023). Modeling and hexahedral meshing of cerebral arterial networks from centerlines. *Medical Image Analysis*, 89, 102912. doi: 10.1016/j.media.2023.102912

[11] Athani, A., Ghazali, N.N.N., Badruddin, I.A., Kamangar, S., Anqi, A.E., & Algahtani, A. (2022). Investigation of two-way fluid-structure interaction of blood flow in a patient-specific left coronary artery. *Bio-Medical Materials and Engineering*, 33(1), 13–30. doi: 10.3233/bme-201171

[12] Yushkevich, P.A., Piven, J., Hazlett, H.C., Smith, R.G., Ho, S., Gee, J.C., & Gerig, G. (2006). User-guided 3D active contour segmentation of anatomical structures: Significantly improved efficiency and reliability. *NeuroImage*, 31(3), 1116–1128. doi: 10.1016/j.neuroimage.2006.01.015

[13] Avants, B.B., Tustison, N.J., Song, G., Cook, P.A., Klein, A., & Gee, J.C. (2011). A reproducible evaluation of ANTs similarity metric performance in brain image registration. NeuroImage, 54(3), 2033–2044. doi: 10.1016/j.neuroimage.2010.09.025

[14] Systems 3D. http://www.geomagic.com/en/products/design/overview [accessed 25 Nov. 2023].

[15] Ansys.com. *Academic Research Fluent, Release 2021R2*. 2021.

[16] Korteweg, D.J. (1878). Ueber die Fortpflanzungsgeschwindigkeit des Schalles in elastischen Röhren. *Annalen Der Physik*, 241(12), 525–542. doi:10.1002/andp.18782411206

[17] Sinek, A., Mesek, M., Rojczyk, M., Juszczyk, J., Adamczyk, W. P., Sturdy, J., Melka, B., Golda, A., Nowok, M., Ostrowski, Z., & Białecki, R. (2023). Evaluating the precision and reproducibility of non-invasive deformation measurements in an arterial phantom. *Measurement: Journal of the International Measurement Confederation*, 216(112904), 112904. doi: 10.1016/j.measurement.2023.112904

[18] Hellmuth R. https://commons.wikimedia.org/w/index.php?curid=54810155 [accessed 25 Nov. 2023].

[19] Painter, P.R., Edén, P., & Bengtsson, H.U. (2006). Pulsatile blood flow, shear force, energy dissipation and Murray's Law. *Theoretical Biology & Medical Modelling*, 3, 31. doi: 10.1186/1742-4682-3-31

[20] Zarins, C.K., Zatina, M.A., Giddens, D.P., Ku, D.N., & Glagov, S. (1987). Shear stress regulation of artery lumen diameter in experimental atherogenesis. *Journal of Vascular Surgery*, 5(3), 413−420. https://pubmed.ncbi.nlm.nih.gov/3509594

[21] Olufsen, M.S., Peskin, C.S., Kim, W.Y., Pedersen, E.M., Nadim, A., & Larsen, J. (2000). Numerical simulation and experimental validation of blood flow in arteries with structured-tree outflow conditions. *Annals of Biomedical Engineering*, 28(11), 1281−1299. doi: 10.1114/1.1326031

[22] Vignon-Clementel, I.E., Figueroa, C.A., Jansen, K.E., & Taylor, C.A. (2006). Outflow boundary conditions for three-dimensional finite element modeling of blood flow and pressure in arteries. *Computer Methods in Applied Mechanics and Engineering*, 195(29−32), 3776–3796. doi: 10.1016/j.cma.2005.04.014

[23] Adji, A., Hirata, K., & O'Rourke, M.F. (2006). Clinical use of indices determined non-invasively from the radial and carotid pressure waveforms. *Blood Pressure Monitoring*, 11(4), 215−221. doi: 10.1097/01.mbp.0000218001.50333.b7

[24] Nelson, M.R., Stepanek, J., Cevette, M., Covalciuc, M., Hurst, R.T., & Tajik, A.J. (2010). Noninvasive measurement of central vascular pressures with arterial tonometry: Clinical revival of the pulse pressure waveform? *Mayo Clinic Proceedings. Mayo Clinic*, 85(5), 460–472. doi: 10.4065/mcp.2009.0336

[25] Ku, D.N., Giddens, D.P., Zarins, C.K., & Glagov, S. (1985). Pulsatile flow and atherosclerosis in the human carotid bifurcation. Positive correlation between plaque location and low oscillating shear stress. *Arteriosclerosis (Dallas, Texas)*, 5(3), 293–302. doi: 10.1161/01.atv.5.3.293

[26] Melka, B., Psiuk-Maksymowicz, K, Borys, D., Ostrowski, Z., Rojczyk, M., Gracka, M., Adamczyk, W.P., & Białecki, R.A. (2023). Numerical modelling of myocardial bridge covering dynamic shape of the human coronary artery (Book of Abstracts, pp. 87). *XXVII Polish Conference on Biocybernetics and Biomedical Engineering*, 27−29 September, Lodz, Poland.

[27] Nader, E., Skinner, S., Romana, M., Fort, R., Lemonne, N., Guillot, N., Gauthier, A., Antoine-Jonville, S., Renoux, C., Hardy-Dessources, M.D., Stauffer, E., Joly, P., Bertrand, Y., & Connes, P. (2019). Blood rheology: Key parameters, impact on blood

flow, role in sickle cell disease and effects of exercise. *Frontiers in Physiology*, 10, . doi: 10.3389/fphys.2019.01329

[28] Wajihah, S.A., & Sankar, D.S. (2023). A review on non-Newtonian fluid models for multi-layered blood rheology in constricted arteries. *Archive of Applied Mechanics*, 93(5), 1771–1796. doi: 10.1007/s00419-023-02368-6

[29] Abbasian, M., Shams, M., Valizadeh, Z., Moshfegh, A., Javadzadegan, A., & Cheng, S. (2020). Effects of different non-Newtonian models on unsteady blood flow hemodynamics in patient-specific arterial models with in-vivo validation. *Computer Methods and Programs in Biomedicine*, 186(105185), 105185. doi: 10.1016/j.cmpb.2019.105185

[30] Bigaj, K., Rojczyk, M., Wasilewski, J., Melka, B., Ostrowski, Z., Gracka, M., Adamczyk, W., & Białecki, R. (2023). CFD assessment of hemodynamics in coronary arteries using three rheological models (in Polish). *Proceedings of the Polish Congress of Rheology*, 18–20 September, Kraków-Wieliczka, Poland.

[31] Liu, J., Yu, F., & Zhang, Y. (2020). MP-PIC simulation of blood cell movement through a LAD with high stenosis. *Powder Technology*, 361, 448–454. doi: 10.1016/j.powtec.2019.05.076

[32] Melka, B., Adamczyk, W.P., Rojczyk, M., Nowak, M.L., Gracka, M., Nowak, A.J., Golda, A., Bialecki, R.A., & Ostrowski, Z. (2019). Numerical investigation of multiphase blood flow coupled with lumped parameter model of outflow. *International Journal of Numerical Methods for Heat and Fluid Flow*, 30(1), 228–244. doi: 10.1108/hff-04-2019-0279

[33] Farina, A., Fasano, A., & Rosso, F. (2023). A theoretical model for the Fåhræus effect in medium–large microvessels. *Journal of Theoretical Biology*, 558, 111355. doi: 10.1016/j.jtbi.2022.111355